# Mechanisms of proton transfer in Nafion®: elementary reactions at the sulfonic acid groups

Kritsana Sagarik,*[ab] Mayuree Phonyiem,[a] Charoensak Lao-ngam[a] and Sermsiri Chaiwongwattana[a]

*Received 29th November 2007, Accepted 17th January 2008*
*First published as an Advance Article on the web 21st February 2008*
**DOI: 10.1039/b718480h**

Proton transfer reactions at the sulfonic acid groups in Nafion® were theoretically studied, using complexes formed from triflic acid ($CF_3SO_3H$), $H_3O^+$ and $H_2O$, as model systems. The investigations began with searching for potential precursors and transition states at low hydration levels, using the test-particle model (T-model), density functional theory (DFT) and *ab initio* calculations. They were employed as starting configurations in Born–Oppenheimer molecular dynamics (BOMD) simulations at 298 K, from which elementary reactions were analyzed and categorized. For the $H_3O^+$–$H_2O$ complexes, BOMD simulations suggested that a quasi-dynamic equilibrium could be established between the Eigen and Zundel complexes, and that was considered to be one of the most important elementary reactions in the proton transfer process. The average lifetime of $H_3O^+$ obtained from BOMD simulations is close to the lowest limit, estimated from low-frequency vibrational spectroscopy. It was demonstrated that proton transfer reactions at $-SO_3H$ are not concerted, due to the thermal energy fluctuation and the existence of various quasi-dynamic equilibria, and $-SO_3H$ could directly and indirectly mediate proton transfer reactions through the formation of proton defects, as well as the $-SO_3^-$ and $-SO_3H_2^+$ transition states.

## 1. Introduction

An energy crisis and environmental concerns about global warming, as well as the need to reduce $CO_2$ emissions, have provided strong motivation to seek ways of improving energy conversion technology. The proton exchange membrane fuel cell (PEMFC) has received much attention as one of the most promising energy suppliers for the future world.[1–3] The polymer electrolyte membrane which has been widely used in PEMFCs is Nafion®, introduced by Dupont in 1967.[2] Nafion® is a perfluorinated polymer with hydrophobic Teflon backbone and randomly attached hydrophilic side chains. The backbones and the side chains of Nafion® are terminated by trifluoromethanesulfonic (triflic) acid, which is known to be one of the strongest acids. The triflic acid functional groups ($-CF_2SO_3H$) are preferentially hydrated and play important roles in proton transfer reactions in PEMFCs. Experiments have shown that hydrated $-CF_2SO_3H$ form aggregates, resulting in large interconnected hydrophilic domains.[4] Since the hydrophilic and hydrophobic domains are quite well separated,[5,6] theoretical and experimental investigations could emphasize only the hydrophilic domains, in which proton conduction takes place. It was observed in general that the degree of hydration at $-CF_2SO_3H$, the morphology of PEM and the size of the hydrophilic domains are directly related to the efficiency of proton conduction in Nafion®.[5,7–9] Although some theoretical and experimental information has been accumulated, the complete mechanisms of proton conduction in Nafion® seem not available, especially at the molecular level.[5,7–9] Since basic chemistry of Nafion® has been discussed in details in many review articles, only some information relevant to the present study will be briefly summarized.

Three basic molecular fragments, potentially involved in proton transfer reactions at the hydrophilic side chains in Nafion®, are $-(CF_2OCF_2)-$, $-CF_2SO_3H$ and $-CF_2SO_3^-$. Density functional theory (DFT) at B3LYP/6-31G(d,p) level[10,11] suggested that, the hydrogen-bond (H-bond) between $CF_3OCF_3$ and $H_2O$ is rather weak, due to the strong electron withdrawing effects from the two $CF_3$ groups. Therefore, $-(CF_2OCF_2)-$ might not be directly involved in proton transfer reactions in Nafion®, which is in accordance with IR experiment[12] and molecular dynamic (MD) simulations.[13] Experimental evidence has shown that when sufficiently hydrated, the $-CF_2SO_3H$ groups in Nafion® are highly dissociated.[14–16] Spectroscopic measurements in which the assignment and comparison of IR and Raman spectra of individual species in Nafion® were made[14,15] revealed that $-CF_2SO_3H$ could be completely dissociated, depending upon the experimental conditions. Dielectric spectroscopy[16] also showed a strong dependence of the dielectric constant and the specific conductivity of Nafion® with water content. Whereas $^{19}F$ NMR experiment[17] indicated that there is a range of temperatures over which the $-CF_2SO_3H$ groups in

[a] *School of Chemistry, Institute of Science, Suranaree University of Technology, Nakhon Ratchasima 30000, Thailand. E-mail: kritsana@sut.ac.th; Fax: (6644) 224635; Tel: (6644) 224635*
[b] *National Nanotechnology Center (NANOTEC), National Science and Technology Development Agency (NSTDA), Pathumthani 12120, Thailand*

 

Nafion® go from being fully dissociated to being fully associated upon cooling.

Attempts have been made to probe the acidity of $CF_3SO_3H$, as well as to determine the transition state ion-pair complex formed from $CF_3SO_3^-$ and $H_3O^+$ in the gas phase.[18] It was reported that, with the inclusion of electrostatic free energy, the activation energy for the deprotonation of $CF_3SO_3H$ amounts to 19.6 kJ mol$^{-1}$, implying that, the ion-pair complex are not stable in the gas phase and some water molecules are required to stabilize both $CF_3SO_3^-$ and $H_3O^+$. Mechanisms of proton dissociation from $CF_3SO_3H$ were examined by Paddison *et al.*,[19,20] by performing a series of B3LYP/6-31G(d,p) calculations on clusters of the $CF_3SO_3H$–$(H_2O)_n$ complexes, $1 \leq n < 6$. Paddison *et al.* reported that, no proton dissociation was observed until three water molecules were included, and $H_3O^+$ could be stabilized through the formation of H-bonds with two water molecules and one oxygen atom of $CF_3SO_3^-$. This H-bond complex could represent one of the precursors for proton dissociation from $CF_3SO_3H$. Interesting results were obtained when up to five water molecules were added, with $H_3O^+$ located progressively further away from $CF_3SO_3^-$, and when six water molecules were added, a complete separation of $H_3O^+$ from $CF_3SO_3^-$ was observed. The results in ref. 19 and 20 suggested a possible scenario for proton dissociation and showed how $H_3O^+$ moves away from $CF_3SO_3^-$.

Mechanisms of proton dissociation at $-CF_2SO_3H$ in minimally hydrated PEM were proposed based on DFT-MD simulations on triflic acid monohydrate solid ($(CF_3SO_3^-H_3O^+)_4$).[21] DFT-MD simulations suggested a relay-type mechanism, in which a proton defect represents an intermediate state; the defect involves formation of the Zundel complex ($H_5O_2^+$) and the reorganization of the neighboring $-CF_2SO_3^-$ groups, which share a proton between the oxygen atoms of the anionic sites. The proposed mechanism also revealed a possibility for proton conduction along the hydrophilic head groups, $-CF_2SO_3H$ and $-CF_2SO_3^-$. The results in ref. 21 are in good agreement with the activation energy for proton transfer in minimally hydrated Nafion® reported in ref. 22.

Similar theoretical studies were carried out on short-side-chain perfluorosulfonic acids, in which large scale DFT geometry optimizations were conducted on fragments of Nafion®, with and without water molecules and with distinct pendant chain separations.[23–25] B3LYP/6-311G(d,p) revealed a possibility for proton transfer between two adjacent hydrophilic groups, along the H-bond networks of water connecting them. The proposed proton transfer pathway is mediated by the formations of the –S–O···H···O–H H-bond, as well as $H_5O_2^+$.[23] It was suggested in ref. 24 and 25 that the number of water molecules required to promote proton dissociation could be reduced when the $-CF_2SO_3H$ groups are brought closer to each other through conformational change in the backbone. These show the importance of side chain flexibility and backbone conformation in proton transfer in short-side-chain perfluorosulfonic acid membranes at low water content.

*Ab initio* calculations and MD simulations on the complexes formed from $CF_3CF_2SO_3H$ and $nH_2O$, $1 \leq n \leq 4$, available to us after the manuscript has been completed, indicated that for $n = 3$, the neutral and ion-pair complexes are close in energy and are accessible in the fluctuation dynamics of proton transport,[26] whereas for $n \leq 2$, the only relevant complex is the neutral form. Most importantly, it was suggested in ref. 26 that, based on the free energy surface for proton exchange, the $CF_3CF_2SO_3H_2^+$–$H_2O$ and $CF_3CF_2SO_3H$–$H_3O^+$ complexes are nearly isoenergetic, and $CF_3CF_2SO_3H_2^+$ could play important roles in proton conduction at low hydration levels.

In the present study, a theoretical method which takes into account the dynamics of formation and cleavage of covalent and H-bonds was employed in the study of proton transfer reactions at a hydrophilic functional group in model Nafion®. While the other theoretical investigations[18–20] focused on conditions and mechanisms of proton dissociation from $-CF_2SO_3H$, as well as proton conduction from the dissociated species ($-CF_2SO_3^-$), the present study emphasized on how $-CF_2SO_3H$ facilitates or mediates transportation of an excess proton. Special attention was given to precursors and transition states, as well as dynamics in elementary reactions. The complexes formed from $CF_3SO_3H$, $H_3O^+$ and $H_2O$ were employed as model systems, from which dynamics of an excess proton and proton defects at and in the vicinity of $-CF_2SO_3H$ was systematically studied. In order to obtain information specifically at $-CF_2SO_3H$, as well as to reduce complexity of H-bonds in the model systems, the present investigations were restricted to reactions at low hydration levels and at short time. Since $H_3O^+$ plays the most important role in proton transfer reactions in aqueous solutions, its basic dynamic information was obtained based on the same approaches, using the complexes formed from $H_3O^+$ and $H_2O$ as model systems. Characteristic proton transfer reactions in the $H_3O^+$–$H_2O$ complexes were described and used in the discussions of the $CF_3SO_3H$–$H_3O^+$–$H_2O$ complexes.

## 2. Computational methods

For hydration of a single proton, according to experimental and theoretical investigations,[27,28] there are at least three important H-bond structures involved in proton transfer reactions, namely, $H_3O^+$, $H_5O_2^+$ and the Eigen complex ($H_9O_4^+$). Based on a neutron diffraction experiment, with hydrogen isotope substitutions and Monte Carlo simulations (MC),[28] the first hydration shell of $H_3O^+$ consists of four water molecules and only three of them strongly H-bond to the hydrogen atoms of $H_3O^+$. *Ab initio* calculations in ref. 29 showed that the fourth water molecule, initially attached to the oxygen atom of $H_3O^+$, eventually moves away to the second hydration shell. Therefore, in the present study, up to three water molecules were considered in the investigation of basic elementary reactions in the proton transfer process at $H_3O^+$.

Since mechanisms of proton conduction in Nafion® are complicated, care must be exercised in selecting model molecules and theoretical methods. Our previous experience on strong H-bond clusters[30–34] showed that some structural and energetic information in the gas phase could provide the basis for discussion in aqueous solutions. Therefore, it was our strategy to explore proton transfer reactions at low hydration levels. Due to the fact that, superacid characters of Nafion® are localized at $-CF_2SO_3H$, the present study concentrated only on reactions among $-CF_2SO_3H$, $H_3O^+$ and $H_2O$, using

the complexes formed from $CF_3SO_3H$, $H_3O^+$ and $H_2O$ as model systems; including $H_3O^+$ in the model systems could promote proton transfer reactions by creating proton defect which involves the formation of $H_5O_2^+$, as in the case of water[35] and triflic acid monohydrate solid.[21] Because the size of the model systems must be reasonable and manageable by our computer resources, the $CF_3SO_3H$–$H_3O^+$–$H_2O$ $1:1:n$ complexes, $1 \leq n \leq 3$, were adopted. It should be added that previous theoretical investigations considered $-CF_2SO_3H$ as a primary source of proton, from which $H_3O^+$ and $-CF_2SO_3^-$ are generated. Therefore, proton transfer reactions among $-CF_2SO_3H$, $H_3O^+$ and $H_2O$ have not been emphasized.

### 2.1 T-model

Since proton transfer reactions have been pointed out to be sensitive to structures and dynamics of the H-bond,[36] all important H-bond structures in the model systems had to be identified, characterized and analyzed. Attention was focused on H-bond structures, which could be precursors or transition states in proton transfer pathways. In order to effectively and systematically scan the potential energy surfaces, T-model potentials were constructed and employed in the calculations of the equilibrium structures of the $H_3O^+$–$H_2O$ and $CF_3SO_3H$–$H_3O^+$–$H_2O$ complexes. Since the T-model had been discussed in details in our previous studies,[30–34,37–41] only some important aspects of geometry optimizations will be briefly summarized.

For the $H_3O^+$–$H_2O$ complexes, a rigid $H_3O^+$ was placed at the origin of the Cartesian coordinate system. The coordinates of water molecules were randomly generated in the vicinity of $H_3O^+$. Based on the T-model potentials, equilibrium structures of the $H_3O^+$–$H_2O$ complexes were searched, using a minimization technique. Similar methods were applied on the $CF_3SO_3H$–$H_3O^+$–$H_2O$ complexes, in which $CF_3SO_3H$ was placed at the origin of the Cartesian coordinate system, and the positions and orientations of $H_3O^+$ and $H_2O$ were randomly assigned in its vicinity. For each H-bond complex, one-hundred starting configurations were generated and employed as starting configurations in the T-model geometry optimizations.

### 2.2 DFT and *ab intio* calculations

Since the T-model potentials are based on rigid molecules, in which cooperative effects are neglected, further structural refinements had to be made using appropriate quantum chemical methods. As it is known in general that sophisticated theoretical methods require more computer resources, and especially in the present case, MD simulations with thousands of timesteps must be performed, it was necessary to compromise between the accuracy of theoretical methods and the available computer resources. A literature survey showed that DFT methods have been frequently chosen due to the ability to treat molecules of relatively large sizes with a reasonable degree of accuracy, compared to other nonempirical methods. Especially for similar H-bond systems,[7,10,11,19,20,23] the DFT method at B3LYP/6-31G(d,p) level represents one of the most popular choices. Therefore, it was adopted as a primary candidate in the refinement of the T-model results. It should be noted, however, that the performance of DFT methods can be poor or fairly good, depending upon the chemical systems considered. As in the present case, the existence of three fluorine atoms in $CF_3SO_3H$ could bring about strong electron correlation effects, and thus made it necessary to examine the applicability of B3LYP/6-31G(d,p) in details. Our experience on strong H-bond systems[30,33,39] suggested that *ab initio* calculations at MP2/6-311++G(d,p) or MP2/6-311++G(2d,2p) level could serve as a benchmark in this case.

The absolute and some local minimum energy geometries of the H-bond complexes, predicted from the T-model potentials, were employed as starting configurations in DFT and *ab initio* geometry optimizations. Both partial and full geometry optimizations were performed, using the Berny algorithm in Gaussian 03.[42] In partial geometry optimizations, monomer geometries were kept constant and only the intermolecular geometrical parameters were optimized. The purpose of the partial geometry optimizations was to verify the T-model optimized geometries, whereas the full geometry optimizations were aimed at structural refinements. In the present study, the partial and full geometry optimizations were denoted by OPT1 and OPT2, respectively. Since forces in MD simulations are computed from energy gradients, which are determined by structures of potential energy surface, and in order to compare the performance among candidate theoretical methods, the potential energy profiles for a single proton transfer event were constructed for selected H-bond complexes, using both DFT and *ab initio* calculations; by moving a proton within a fixed H-bond distance. In the present case, B3LYP/6-31G(d,p), HF/6-311++G(d,p) and MP2/6-311++G(d,p) calculations were employed in the calculations of the potential energy profiles. For the DFT method, additional calculations at B3LYP/6-31+G(d,p) level were made to examine the effects of diffuse functions.

### 2.3 MD simulations

The dynamics of rapid covalent and H-bond formation and cleavage could be studied reasonably well using theoretical approaches that incorporate quantum chemical methods into MD simulations,[43] among which DFT-MD simulations have been widely used in recent years.[44,45]

In the present work, the precursors and transition states, as well as elementary reactions, in proton transfer processes at $-CF_2SO_3H$ were studied using Born–Oppenheimer MD (BOMD) simulations.[46,47] Within the framework of BOMD simulations, classical equations of motions of nuclei on the Born–Oppenheimer surfaces are integrated, whereas forces on nuclei are calculated in each MD step from quantum energy gradients, with the molecular orbitals (MOs) updated by solving Schroedinger equations in the Born–Oppenheimer approximation. This makes BOMD simulations more accurate, as well as considerably CPU time consuming, compared to conventional classical MD simulations, in which forces on nuclei are determined from predefined empirical or quantum pair potentials. It should be noted that the high mobility of the excess proton was initially attributed to QM tunneling.[48] This has been challenged, for example, by the results obtained from *ab initio* BOMD simulations[36] and conductivity

measurements,[49] which showed that proton transfer reaction mechanisms could be explained reasonably well without assuming the proton tunneling to be the important pathway.

Since proton conduction, especially in aqueous solutions, involves dynamic processes with different timescales,[35,50,51] the complexity of proton transfer reactions could be reduced using various approaches. The observation that the actual proton transfer occurs on a femtosecond (fs) timescale,[51] which is in general faster than solvent reorganization,[50] made it reasonable to perform BOMD simulations by focusing only on short-lived phenomena which take place before or after major H-bond structure reorganizations. To ensure that all important dynamics was taken into account, several BOMD trajectories were generated at 298 K, starting from the equilibrium structures of the $H_3O^+$–$H_2O$ and $CF_3SO_3H$–$H_3O^+$–$H_2O$ complexes computed in the previous sections. Since in aqueous solutions, rapid interconversion between the Zundel and Eigen complexes happens within about 100 fs ($10^{-13}$ s),[35] the time-step used in solving dynamic equations was set to 0.5 fs. In each BOMD simulation, 500 fs was spent on equilibration, after which 2000 fs was devoted to property calculations.

Since correlation exists between proton conductivity and H-bond structure,[35] JMOL[52] was employed to visualize molecular motions in the course of BOMD simulations. In addition, BOMD trajectories were analyzed in details by monitoring fluctuations and changes in H-bond structures; some characteristic H-bond distances were plotted with MD simulation time. For example, the Oh···Ow, Ow–Hw and Oh–Hh distances were plotted with MD simulation time to study the dynamics in the Zundel and Eigen complexes; h = hydronium ion and w = water. The plots were regarded as proton transfer profiles in the present work. In combination with the molecular motions displayed by JMOL, precursors, transition states and the elementary reactions in proton transfer processes were analyzed and categorized. The average lifetimes of the precursors, transition states and products were roughly estimated from the proton transfer profiles and further analyzed in details. The analyses of the proton transfer profiles will be discussed in the forthcoming sections.

## 3. Results and discussion

### 3.1 Structures and energetic

The absolute and some lowest-lying minimum energy geometries of the H-bond complexes, together with corresponding interaction energies and characteristic H-bond distances, are displayed in Tables 1 and 2, as well as Fig. 1 and 2.

**3.1.1 The $H_3O^+$–$H_2O$ complexes.** For the $H_3O^+$–$H_2O$ 1 : $n$ complex, $1 \leq n \leq 3$, T-model, DFT and *ab initio* geometry optimizations suggested only one predominant H-bond structure; $H_3O^+$ acts as proton donor towards $H_2O$, structures **a**, **b** and **c** in Table 1. DFT and *ab initio* calculations with partial geometry optimizations predicted the same structures as the T-model. The Zundel complex, in which a hydrogen atom is equally shared between two water molecules and considered as a defect in the H-bond network,[21] was obtained when DFT and *ab initio* calculations with full geometry optimizations being applied. The Oh···H···Ow and Oh···H distances derived from B3LYP-OPT2 and MP2-OPT2 are almost the same, about 2.4 and 1.2 Å, respectively. The extraordinary short H-bond distance, as in the case of the Zundel complex, could be related to a high possibility for proton transfer and, therefore, used as a criterion to monitor proton transfer reactions.[35]

Similar trends were observed in the $H_3O^+$–$H_2O$ 1 : 2 complexes. T-model, DFT and *ab initio* calculations with partial geometry optimizations predicted the structure with two

**Table 1** Structures of the $H_3O^+$–$H_2O$ complexes, obtained from the T-model, DFT and *ab initio* geometry optimizations. (a) $H_3O^+$–$H_2O$ 1 : 1 complex. (b) $H_3O^+$–$H_2O$ 1 : 2 complex. (c) $H_3O^+$–$H_2O$ 1 : 3 complex

| | Method | $\Delta E$/kJ mol$^{-1}$ | Oh–Hh···Ow/Å | Oh–Hh–Ow/° |
|---|---|---|---|---|
| (a) 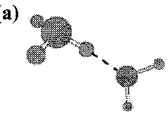 | T-model | −117.5 | 2.51 | 151.0 |
| | MP2-OPT1 | −135.5 | 2.46 | 175.9 |
| | MP2-OPT2 | — | 2.39[a] | 174.0 |
| | B3LYP-OPT1 | −160.7 | 2.43 | 174.5 |
| | B3LYP-OPT2 | — | 2.40[a] | 174.2 |
| (b) 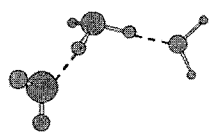 | T-model | −229.9 | 2.52 | 152.6 |
| | MP2-OPT1 | −244.5 | 2.52 | 174.3 |
| | MP2-OPT2 | — | 2.50 | 175.5 |
| | B3LYP-OPT1 | −287.6 | 2.49 | 174.0 |
| | B3LYP-OPT2 | — | 2.47 | 174.6 |
| (c) 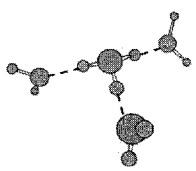 | T-model | −334.4 | 2.58 | 171.7 |
| | MP2-OPT1 | −334.0 | 2.57 | 175.6 |
| | MP2-OPT2 | — | 2.57 | 175.9 |
| | B3LYP-OPT1 | −388.4 | 2.54 | 176.7 |
| | B3LYP-OPT2 | — | 2.55 | 175.5 |

[a] The Zundel complex; an excess proton equally shared between two water molecules. MP2-OPT1 = MP2/6-311++G(2d,2p) with partial geometry optimizations. MP2-OPT2 = MP2/6-311++G(2d,2p) with full geometry optimizations. B3LYP-OPT1 = B3LYP/6-31G(d,p) with partial geometry optimizations. B3LYP-OPT2 = B3LYP/6-31G(d,p) with full geometry optimizations.

**Table 2** Structures of the $CF_3SO_3H$–$H_2O$ and $CF_3SO_3H$–$H_3O^+$ 1 : 1 complexes, obtained from the T-model, DFT and *ab initio* geometry optimizations. (a)–(c) $CF_3SO_3H$–$H_2O$ 1 : 1 complexes. (d) $CF_3SO_3H$–$H_3O^+$ 1 : 1 complex

| | | Method | $\Delta E$/kJ mol$^{-1}$ | H-bond | Distance/Å | Angle/° |
|---|---|---|---|---|---|---|
| (a) | 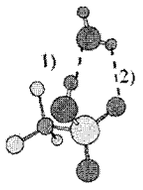 | T-model | −51.9 | (1) O–H···Ow | 2.71 | 158.4 |
| | | | | (2) Ow–Hw···O | 2.79 | 111.6 |
| | | MP2-OPT1 | −51.9 | | 2.68 | 166.2 |
| | | | | | 2.93 | 133.3 |
| | | B3LYP-OPT2 | — | | 2.60 | 166.4 |
| | | | | | 2.84 | 127.2 |
| (b) | 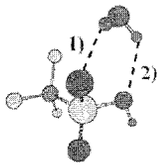 | T-model | −15.7 | (1) Ow–Hw···O | 2.95 | 122.8 |
| | | | | (2) Ow–Hw···O | 3.05 | 127.6 |
| | | MP2-OPT1 | −13.2 | | 3.18 | 134.5 |
| | | | | | 3.20 | 136.3 |
| | | B3LYP-OPT2 | — | | 3.01 | 138.9 |
| | | | | | 3.22 | 102.3 |
| (c) | 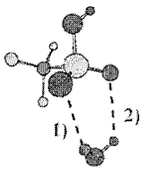 | T-model | −15.7 | (1) Ow–Hw···O | 2.95 | 122.8 |
| | | | | (2) Ow–Hw···O | 3.05 | 127.6 |
| | | MP2-OPT1 | −13.2 | | 3.21 | 127.5 |
| | | | | | 3.24 | 123.6 |
| | | B3LYP-OPT2 | — | | 3.10 | 120.7 |
| | | | | | 3.08 | 120.1 |
| (d) | 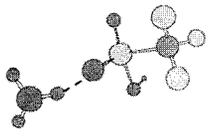 | T-model | −68.1 | Oh–Hh···O | 2.60 | 141.3 |
| | | MP2-OPT1 | −114.6 | | 2.48 | 177.3 |
| | | B3LYP-OPT2 | — | | 2.40 | 177.4 |

MP2-OPT1 = MP2/6-311++G(d,p) with partial geometry optimizations. B3LYP-OPT2 = B3LYP/6-31G(d,p) with full geometry optimizations.

equivalent linear Oh–Hh···Ow H-bonds to be the most stable. Only slightly shorter Oh–Hh···Ow H-bond distances were observed when MP2-OPT2 and B3LYP-OPT2 were applied on the T-model results. All theoretical methods predicted longer Oh–Hh···Ow H-bond distances when the number of water molecule was gradually increased from one to three. For the $H_3O^+$–$H_2O$ 1 : 3 complex, the T-model suggested the Oh–Hh···Ow H-bond distance to be 2.58 Å, whereas the values obtained from MP2-OPT1 and B3LYP-OPT1 are 2.57 and 2.54 Å, respectively. MP2-OPT2 and B3LYP-OPT2 showed the same trend, with slightly shorter Oh–Hh covalent bonds in $H_3O^+$.

As mentioned earlier, H-bonds in the $H_3O^+$–$H_2O$ complexes have been extensively studied using both experimental and theoretical treatments. It was generally concluded that the introduction of an extra proton to the cluster of water molecules in the gas phase or liquid water results in contraction of H-bonds, through the formation of proton defect which involves $H_5O_2^+$.[35] The isolated $H_5O_2^+$ was reported to possess a very short H-bond distance, approximately 2.4 Å.[36,51,53,54] This is confirmed by all theoretical results obtained here. Both experiments and theories suggested the same trends when water molecules are added to $H_5O_2^+$, namely, the central H-bond in $H_5O_2^+$ is weakened to some extent, leading to relaxation of H-bonds. The H-bond distance in the Eigen complex was reported to be about 2.6 Å,[35,36,51] which is in excellent agreement with the present results.

**3.1.2 The $CF_3SO_3H$–$H_2O$ and $CF_3SO_3H$–$H_3O^+$ complexes.** For the $CF_3SO_3H$–$H_2O$ 1 : 1 complex, T-model, MP2-OPT1 and B3LYP-OPT2 predicted a cyclic H-bond structure in which $CF_3SO_3H$ acts simultaneously as proton donor and acceptor, to be the global minimum energy geometry, structure **a** in Table 2; whereas other cyclic H-bond structures, in which $CF_3SO_3H$ acts only as proton acceptor, structures **b** and **c**, possess considerably lower stability. For the $CF_3SO_3H$–$H_3O^+$ 1 : 1 complex, both the T-model and MP2-OPT1 predicted $H_3O^+$ to be a stronger proton donor than $CF_3SO_3H$, structure **d** in Table 2. The linear H-bond in structure **d** did not change substantially when B3LYP-OPT2 was applied. However, small but not negligible change was observed at the Oh–Hh···O H-bond. It becomes shorter and comparable with the Ow···H···Ow H-bond distance in the Zundel complex. The decrease in the H-bond distance is accompanied by an increase in the Oh–Hh covalent bond distance. This reflects a tendency for proton transfer from $H_3O^+$ to $CF_3SO_3H$, leading to a Zundel-like structure ($CF_3SO_3H_2^+$–$H_2O$) as proposed in ref. 26.

**3.1.3 $CF_3SO_3H$–$H_3O^+$–$H_2O$ complexes.** For the $CF_3SO_3H$–$H_3O^+$–$H_2O$ 1 : 1 : 1 complexes, the T-model generated three important minimum energy geometries, namely, structures **a**, **b** and **c** in Fig. 1. All of them adopt compact cyclic H-bond structures. The most stable one, structure **a**,

 

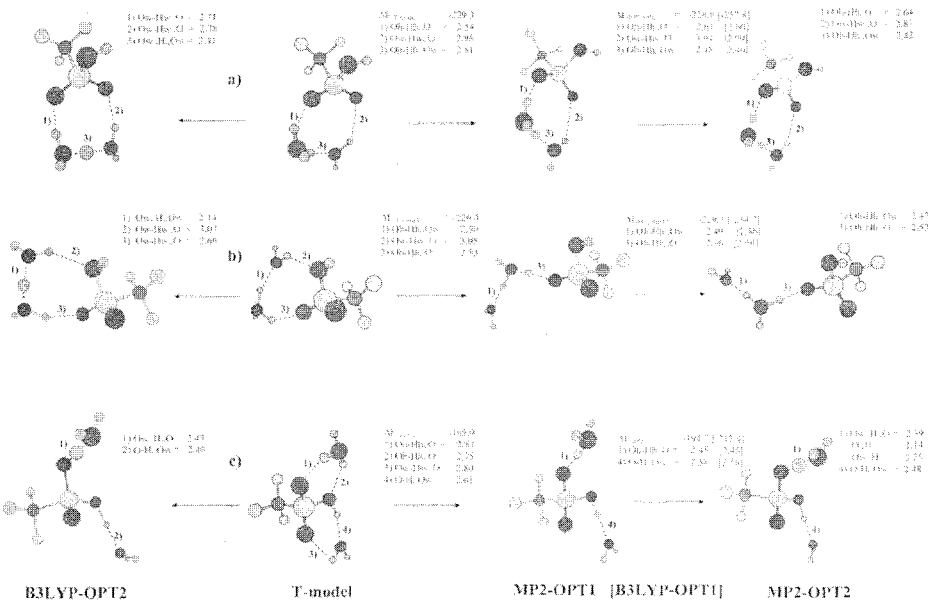


**Fig. 1** Equilibrium structures of the $CF_3SO_3H$–$H_3O^+$–$H_2O$ 1 : 1 : 1 complexes, obtained from the T-model, DFT and *ab initio* geometry optimizations. Interaction energy is given in kJ mol$^{-1}$, angle in degrees and distance in Å. MP2-OPT1 = MP2/6-311++G(d,p) with partial geometry optimizations. MP2-OPT2 = MP2/6-311++G(d,p) with full geometry optimizations. B3LYP-OPT1 = B3LYP/6-31G(d,p) with partial geometry optimizations. B3LYP-OPT2 = B3LYP/6-31G(d,p) with full geometry optimizations. [..] = Values obtained from B3LYP-OPT1.

consists of three H-bonds; $H_3O^+$ and $H_2O$ act as proton donors towards two oxygen atoms of $CF_3SO_3H$. The stability of structure **b** is slightly lower than structure **a** and structure **c** is quite different from structures **a** and **b**. In structure **c**, $CF_3SO_3H$ forms two separate cyclic H-bonds with $H_3O^+$ and $H_2O$. Both are located on the opposite sides of $-SO_3H$. Some H-bonds in structures **b** and **c** were disrupted when MP2-OPT1 and B3LYP-OPT1 were applied on the T-model results, leading to linear H-bond structures. The comparison of the MP2-OPT1 and MP2-OPT2 results in details reveals the important trend; full geometry optimizations lead to shorter H-bond distances, especially where proton transfer could take place, *e.g.* the Oh–Hh···Ow H-bonds in structures **a** and **b**, as well as the Oh–Hh···O H-bonds in structures **b** and **c**. The latter reflect the possibility for proton transfer from $H_3O^+$ to $-SO_3H$, forming the previously proposed $CF_3SO_3H_2^+$ transition state. Starting from the T-model results, B3LYP-OPT2 did not bring about a significant change in the H-bond structures. However, the possibilities for proton transfer in structures **a**, **b** and **c** become more evident. Compared with B3LYP-OPT1, all the H-bonds susceptible to proton transfer are systematically shorter, with hydrogen atoms located nearer to the centers.

Since important information on theoretical methods had already been obtained, it was reasonable to investigate the $CF_3SO_3H$–$H_3O^+$–$H_2O$ 1 : 1 : 2 complex using only the T-model, MP2-OPT2 and B3LYP-OPT2. The T-model predicted four important cyclic H-bond structures in Fig. 2. The most stable one consists of a basic unit similar to structure **a** in the $CF_3SO_3H$–$H_3O^+$–$H_2O$ 1 : 1 : 1 complex, with the second water molecule hydrates at $H_3O^+$. The stability of structure **b** is slightly lower than that in structure **a**. In structure **b**, both $CF_3SO_3H$ and $H_3O^+$ act as proton donors towards water molecules, and the second water molecule hydrates directly at $H_3O^+$. The stability of structures **a** and **b** seems to result from a complete H-bond formation at $H_3O^+$. Structures **c** and **d** are quite different from structures **a** and **b**; only two Oh–Hh covalent bonds in $H_3O^+$ are H-bonded. Comparison of interaction energies ($\Delta E_{T-model}$) suggested that the formation of a large cyclic H-bond tends to reduce the stability of the $CF_3SO_3H$–$H_3O^+$–$H_2O$ 1 : 1 : 2 complexes. The T-model results did not change significantly when B3LYP-OPT2 and MP2-OPT2 were applied, except for structures **c** and **d**, B3LYP-OPT2 showed a higher possibility for the Zundel complex formation. In summary, for the $CF_3SO_3H$–$H_3O^+$–$H_2O$ 1 : 1 : 2 complexes, structures **a**, **b** and **d** reveal possibilities for proton transfer along the H-bond networks connecting the oxygen atoms of $-SO_3H$, whereas structure **c** shows a possibility for proton transfer through $-SO_3H$, *e.g.*, a protonation at one oxygen atom followed by a deprotonation at the O–H group, or *vice versa*. This direct involvement of $-SO_3H$ in proton transfer is similar to the Grotthuss mechanism.[55] In the present case, a relay-type mechanism, in which a proton hops across $-SO_3H$, could take place through the formation of either $-SO_3H_2^+$ or $-SO_3^-$. It should be noted that, although a limited number of H-bond structures was considered in ref. 26, $-SO_3H_2^+$ was recognized in *ab initio* calculations and MD simulations, and pointed out to play important roles in proton transfer at low hydration levels. This was further investigated in our MD simulations in the next sections.

For the $CF_3SO_3H$–$H_3O^+$–$H_2O$ 1 : 1 : 3 complex, both linear and cyclic H-bonds were found in the optimized geometry, structure **e** in Fig. 2. The T-model, MP2-OPT2 and B3LYP-OPT2 predicted a similar trend, namely, all H-bonds susceptible for proton transfer possess short H-bond distances. MP2-OPT2 and B3LYP-OPT2 also showed a possibility to form

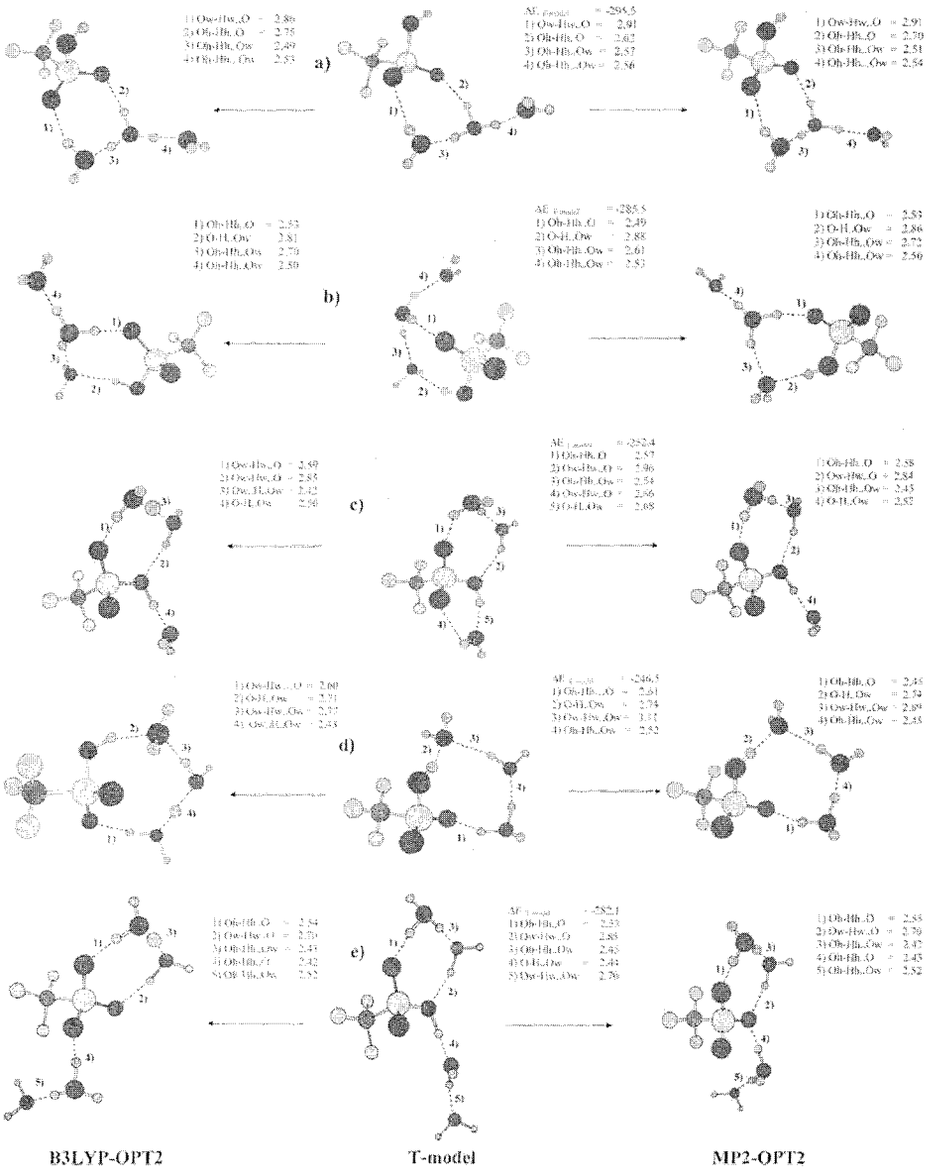


**Fig. 2** Equilibrium structures of the $CF_3SO_3H$–$H_3O^+$–$H_2O$ 1 : 1 : 2 and 1 : 1 : 3 complexes, obtained from the T-model, DFT and *ab initio* calculations. Interaction energy in kJ mol$^{-1}$ and distance in Å. (a)–(d) $CF_3SO_3H$–$H_3O^+$–$H_2O$ 1 : 1 : 2 complexes. (e) $CF_3SO_3H$–$H_3O^+$–$H_2O$ 1 : 1 : 3 complex. MP2-OPT2 = MP2/6-311++G(d,p) with full geometry optimizations. B3LYP-OPT2 = B3LYP/6-31G(d,p) with full geometry optimizations.

$-SO_3^-$, $H_3O^+$ and $H_5O_2^+$ within the $CF_3SO_3H$–$H_3O^+$–$H_2O$ 1 : 1 : 3 complex. The appearance of $-SO_3^-$ and the ion-pair complex when $n = 3$ is in good agreement with the theoretical results in ref. 26.

Comparison of the size and shape of the potential energy profiles for proton transfer in Fig. 3a to 3d revealed that B3LYP/6-31G(d,p), B3LYP/6-31+G(d,p) and MP2/6-311++G(d,p) yield similar trends; whereas HF/6-311++G(d,p) shows different results, *e.g.* the minima are seen systematically at shorter distances. The discrepancies are quite obvious in Fig. 3b to 3e; double-well potential is seen in the case of large cyclic H-bond of water; shoulders are seen in the case of $CF_3SO_3H$–$H_3O^+$–$H_2O$ 1 : 1 : 1 complexes. Based on the above discussions and the fact that DFT requires lowest computational resources, we concluded that B3LYP/6-31G(d,p) is the most appropriate choice for our MD simulations.

### 3.2 Dynamics and elementary reactions

**3.2.1 The $H_3O^+$–$H_2O$ complexes.** Since H-bond structures can vary in a rather wide range, care must be exercised in the discussion of proton transfer profiles. In order to study dynamics and elementary reactions in proton transfer processes, some characteristic structures in proton transfer profiles have to be interpreted, using BOMD results on the $H_3O^+$–$H_2O$ 1 : 1 complex in Fig. 4 and 5 as examples. It appeared, in general, that the proton transfer in $H_5O_2^+$

 

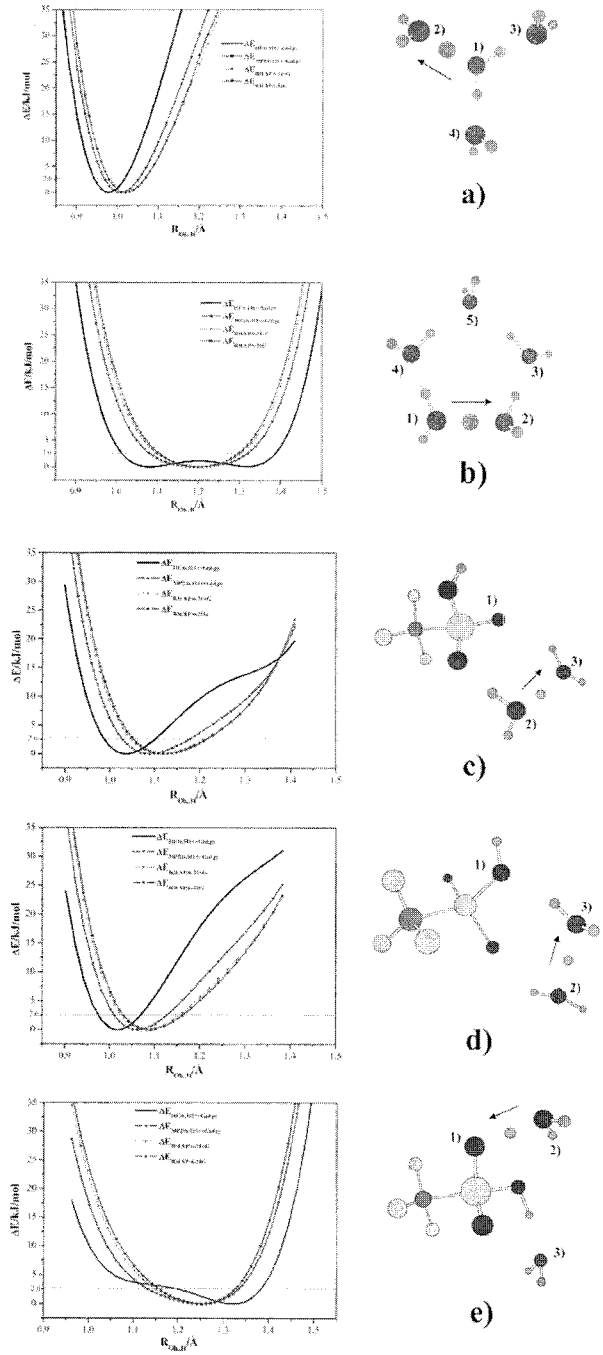

**Fig. 3** Potential energy profiles for single proton transfer, obtained from various theoretical methods. Interaction energy in kJ mol$^{-1}$ and distance in Å. All minima on the potential energy curves were moved to zero for comparison. (a) $H_3O^+$–$H_2O$ 1 : 3 complex. (b) $H_3O^+$–$H_2O$ 1 : 4 complex. (c)–(e) $CF_3SO_3H$–$H_3O^+$–$H_2O$ 1 : 1 : 1 complexes.

depends strongly on the Oh–Hh···Ow H-bond distance, as well as its vibrational amplitude. Examples of two extreme cases, namely, large- and small-amplitude vibrations, are shown in Fig. 4a and 4b, respectively. In order to simplify the discussion, the proton transfer profiles are divided into panels, labeled as $\mathbf{P_1}$, $\mathbf{P_2}$, $\mathbf{P_3}$,..., $\mathbf{P_n}$, respectively.

For large-amplitude vibration, the Oh–Hh···Ow H-bond distance (O1–O2 in Fig. 4a) varies in quite a wide range, from its equilibrium to about 3 Å. A periodic series, consisting of a quasi-dynamic equilibrium followed by an actual proton transfer, was observed in the course of BOMD simulations and could be considered as a part of proton transfer reaction mechanism. For $H_5O_2^+$, the quasi-dynamic equilibrium is characterized by a proton shuttling back and forth in a narrow range within the H-bond, before the actual proton transfer takes place, either in the forward or reverse direction. In Fig. 4a, for example, a quasi-dynamic equilibrium is seen in panel $\mathbf{P_2}$, preceding the actual proton transfer in the forward direction at $t_3 = 2341$ fs. The actual proton transfers are also seen at $t_1 = 2228$ fs, $t_2 = 2317$ fs and $t_4 = 2419$ fs. The lifetime of the quasi-dynamic equilibrium ($\tau_{H_5O_2^+}^{I,ABC}$) could be approximated from the width of panel $\mathbf{P_2}$, and the lifetimes of $H_3O^+$, $\tau_{H_5O_2^+}^{I.C}$ and $\tau_{H_5O_2^+}^{I.A}$, from panels $\mathbf{P_1}$ and $\mathbf{P_3}$, respectively; the former is 24 fs and the latter are 89 and 78 fs, respectively. The superscripts **A** and **C** in $\tau_{H_5O_2^+}^{I.C}$ and $\tau_{H_5O_2^+}^{I.A}$ represent the H-bond structures in Fig. 4c, and I, the elementary reaction in Fig. 5. The superscript **ABC** in $\tau_{H_5O_2^+}^{I,ABC}$ denotes the quasi-dynamic equilibrium established among structures **A**, **B** and **C**. Similar notations will be applied in the forthcoming discussions. Since $\tau_{H_5O_2^+}^{I.A}$ and $\tau_{H_5O_2^+}^{I.C}$ are longer than $\tau_{H_5O_2^+}^{I,ABC}$, the lifetimes of the precursor $H_3O^+$ could be approximated as the rate-determining step for a proton transfer reaction *via* large amplitude vibration in $H_5O_2^+$.

For small-amplitude vibration, the Oh–Hh···Ow H-bond distance (O1–O2 in Fig. 4b) varies in a narrow range near its equilibrium, between 2.3 and 2.7 Å. In this case, proton exchange between two water molecules takes place more often and quite randomly. For example, in Fig. 4b, $\tau_{H_5O_2^+}^{I.A}$ and $\tau_{H_5O_2^+}^{I.C}$ vary from 19 to 39 fs, and up to three actual proton transfers occur between $t_1$ and $t_4$. Interestingly, the O1–O2 vibration starts to damp at $t_1 = 1941$ fs, until a quasi-dynamic equilibrium, with $\tau_{H_5O_2^+}^{I,ABC} = 23$ fs, is reached at $t_5 = 2046$ fs; followed by a proton transfer at $t_6 = 2069$ fs. It should be noted that, although the lifetimes of the precursor $H_3O^+$ ($\tau_{H_5O_2^+}^{I,A}$) for large- and small-amplitude vibrations are somewhat different, $\tau_{H_5O_2^+}^{I,ABC}$ are quite similar.

It could be recognized that proton transfers in $H_5O_2^+$ are activated, when the Oh–Hh···Ow H-bond distance (O1–O2 in Fig. 4a and 4b) is close to its equilibrium, shorter than 2.4 Å, and only one actual proton transfer takes place for each large-amplitude vibration cycle. Therefore, maximum proton transfer cycle time ($\tau_{H_5O_2^+}^{I,PTmax}$) could be defined from large-amplitude vibration; from the time intervals between successive minima of the Oh–Hh···Ow H-bond distance. The proton transfer profiles in Fig. 4a and 4b also revealed that, for large-amplitude vibration, the O1–O2 and O1–$H_1$* motions in panel $\mathbf{P_1}$, as well as the O1–O2 and O2–$H_1$* motions in panel $\mathbf{P_3}$, are correlated, except during the quasi-dynamic equilibrium in $\mathbf{P_2}$; whereas, for small-amplitude vibration, for which proton vibrates with higher frequency, such correlation seems missing. Since the abnormal proton mobility in water has been pointed out to relate to incoherent effects,[50] it is reasonable to approximate the degree of coherence in the H-bond. Similar to statistics and electromagnetic waves, the degree of coherence in the present study should measure the extent of correlation between vibrational motions in the H-bonds, *e.g.* between the

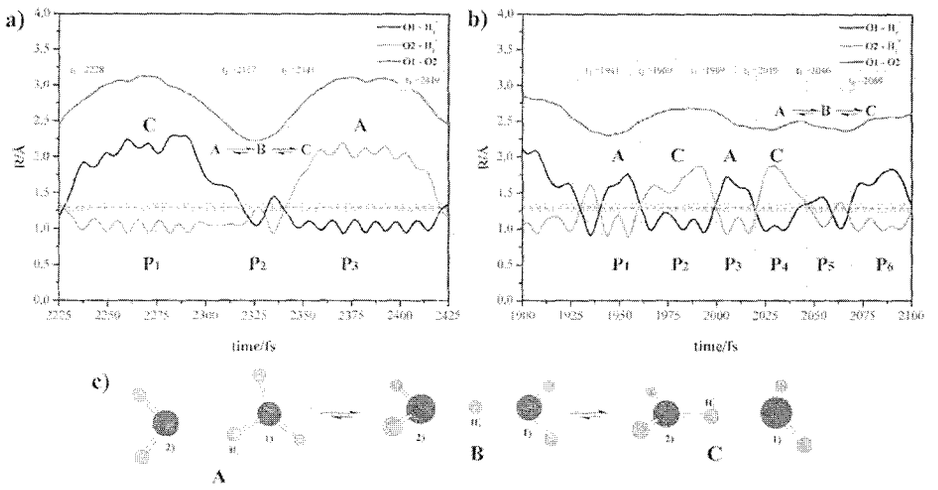


**Fig. 4** Examples of characteristic proton transfer profiles for the $H_3O^+$–$H_2O$ 1 : 1 complex, with snapshots of H-bond structures obtained in the course of BOMD simulations. (a) Large-amplitude vibrations. (b) Small-amplitude vibrations (c) Snapshots of H-bond structures.

O–O and O–H vibrations. Since, for large-amplitude vibration, $\tau_{H_5O_2^+}^{I,A}$ and $\tau_{H_5O_2^+}^{I,PTmax}$ are nearly the same, $\tau_{H_5O_2^+}^{I,A}/\tau_{H_5O_2^+}^{I,PTmax}$ could be adopted as a criterium to measure the degree of coherence ($g_{H_5O_2^+}^{I}$). Therefore, in Fig. 4a, $g_{H_5O_2^+}^{I} \approx 1$ is attributed to the highest degree of coherence; whereas in Fig. 4b, the short lifetimes of the precursor $H_3O^+$ ($\tau_{H_5O_2^+}^{I,A}$ and $\tau_{H_5O_2^+}^{I,C}$) compared to $\tau_{H_5O_2^+}^{I,PT_{max}}$ reflect a lower degree of coherence and higher frequency of proton transfer.

Proton transfer elementary reactions in the $H_3O^+$–$H_2O$ 1 : $n$ complexes, $1 \leq n \leq 3$, are listed in Fig. 5. BOMD simulations predicted the average lifetimes of the quasi-dynamic equilibria in $H_5O_2^+$ ,$\langle\tau_{H_5O_2^+}^{I,AB}\rangle$, $\langle\tau_{H_5O_2^+}^{I,BC}\rangle$ and $\langle\tau_{H_5O_2^+}^{I,ABC}\rangle$, to be 20.5, 19.4 and 15.5 fs, respectively, whereas the average lifetimes of the precursor and product $H_3O^+$, $\langle\tau_{H_5O_2^+}^{I,A}\rangle$ and $\langle\tau_{H_5O_2^+}^{I,C}\rangle$, are nearly the same, 12.4 and 10.7 fs, respectively. The average maximum proton transfer cycle time ($\langle\tau_{H_5O_2^+}^{I,PT_{max}}\rangle$) in this case amounts to 69.9 fs, with $g_{H_5O_2^+}^{I} = 0.2$. This confirms that, on average, small-amplitude vibration with a low degree of coherence dominates in $H_5O_2^+$. Due to the fact that BOMD simulations were started from minimum energy geometries, it was not straightforward to predict the preferential proton transfer directions. However, for each proton transfer elementary reaction, the probability

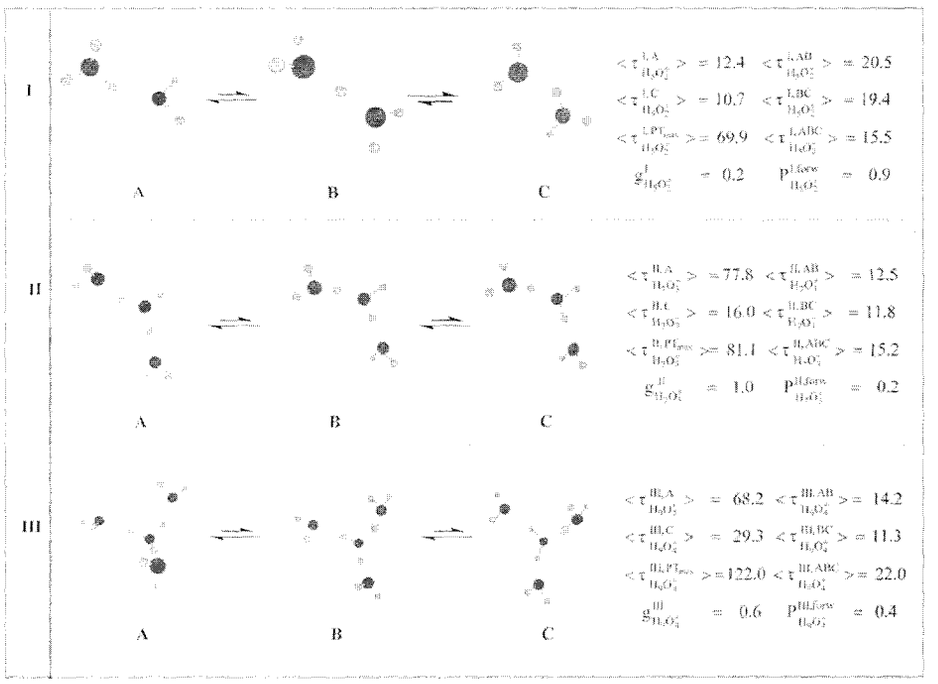


**Fig. 5** Important elementary reactions in proton transfer in the $H_3O^+$–$H_2O$ complexes obtained from BOMD simulations. The symbols are explained in details in the text.

 

for proton transfer in the forward direction ($P_{H_5O_2^+}^{I,forw}$) could be conceivably associated with the average lifetime of the product, which becomes a precursor in the next proton transfer step. Therefore, $P_{H_5O_2^+}^{I,forw}$ was approximated as $\langle\tau_{H_5O_2^+}^{I,C}\rangle/\langle\tau_{H_5O_2^+}^{I,A}\rangle$. Since the product and precursor are the same in $H_5O_2^+$, $P_{H_5O_2^+}^{I,forw} = 1$ represents the upper limit of the relative probability for proton transfer in the forward direction.

The characteristics of proton transfer profiles for the $H_3O^+$–$H_2O$ 1 : 2 complex ($H_7O_3^+$) are not substantially different from $H_5O_2^+$. The presence of another strong Oh–Hh···Ow H-bond in $H_7O_3^+$ tends to increase the stability of the central $H_3O^+$. Since BOMD results in Fig. 5 suggested that $\langle\tau_{H_7O_3^+}^{II,A}\rangle$ and $\langle\tau_{H_7O_3^+}^{II,PT_{max}}\rangle$ are comparable, one could conclude that the elementary reaction **II** favors large-amplitude vibration, with $g_{H_7O_3^+}^{II} \approx 1$, compared to 0.2 in $H_5O_2^+$; $\langle\tau_{H_7O_3^+}^{II,PT_{max}}\rangle$ and $\langle\tau_{H_7O_3^+}^{II,A}\rangle$ are 81.1 and 77.8 fs, respectively. In this case, the relative probability for proton transfer in the forward direction ($P_{H_7O_3^+}^{II,A} = \langle\tau_{H_7O_3^+}^{II,C}\rangle/\langle\tau_{H_7O_3^+}^{II,A}\rangle = 0.2$) is considerably lower than $H_5O_2^+$. The increase in the stability of the central $H_3O^+$ is accompanied by shorter average lifetimes of the quasi-dynamic equilibrium; $\langle\tau_{H_7O_3^+}^{II,AB}\rangle$ and $\langle\tau_{H_7O_3^+}^{II,BC}\rangle$ are 12.5 and 11.8 fs, respectively.

Due to coupled motions among the three strong Oh–Hh···Ow H-bonds, as well as some H-bond structure reorganizations, proton transfer profiles for the $H_3O^+$–$H_2O$ 1 : 3 complex are more complicated than $H_5O_2^+$ and $H_7O_3^+$. Although the central $H_3O^+$ in the Eigen complex ($H_9O_4^+$) is more stabilized than in $H_7O_3^+$, the fluctuations of the surrounding water dipoles seem to help promote proton transfer reactions; similar to an extended local dynamic disorder which leads to a compression and breaking of H-bonds, as discussed in ref. 56. BOMD results suggested two important precursors for proton transfer elementary reactions in the $H_3O^+$–$H_2O$ 1 : 3 complex, namely, the Eigen complex and a linear H-bond structure. Since the proton transfer profiles for the linear H-bond structure are similar to those in $H_7O_3^+$, attention was focused on the Eigen complex. For elementary reaction **III** in Fig. 5, both large- and small-amplitude vibrations were observed in the course of BOMD simulations. Analyses of proton transfer profiles revealed that, due to the coupled vibrational motions, the average lifetime of the central $H_3O^+$ ($\langle\tau_{H_9O_4^+}^{III,A}\rangle$) is shorter than in $H_7O_3^+$ ($\langle\tau_{H_7O_3^+}^{II,A}\rangle$), but still considerably longer than $H_5O_2^+$ ($\langle\tau_{H_5O_2^+}^{I,A}\rangle$), 68.2, 77.8 and 12.4 fs, respectively. For the Eigen complex, the average maximum proton transfer cycle time ($\langle\tau_{H_9O_4^+}^{III,PT_{max}}\rangle$ = 122.0 fs) is nearly twice longer than the average lifetime of the precursor ($\langle\tau_{H_9O_4^+}^{III,A}\rangle$ = 68.2 fs). This implies that, on average, the probabilities for proton transfers through small- and large-amplitude vibrations are comparable; $g_{H_9O_4^+}^{III} = 0.6$ and $P_{H_9O_4^+}^{III,forw} = \langle\tau_{H_9O_4^+}^{III,C}\rangle/\langle\tau_{H_9O_4^+}^{III,A}\rangle = 0.4$. The former is lower than $H_7O_3^+$, but still higher than $H_5O_2^+$, whereas the latter could support the previous investigation that the proton transfer rate is about one order of magnitude lower than the O–O vibration rate.[56] Since small-amplitude vibration is a characteristic of the Zundel complex, one could conclude that, due to the thermal energy fluctuation and the coupled motions among H-bonds, a quasi-dynamic equilibrium between the Eigen and Zundel complexes could be established in the course of BOMD simulations, and considered as the most fundamental elementary reaction in proton transfer process.

The most important property of $H_3O^+$, which could be obtained from experiments, is the average lifetime. Based on an approximate Eigen's relationship, the average lifetime of $H_3O^+$ was demonstrated to be sensitive to the concentration of acid;[57] as the concentration of the acid increases, so does the average lifetime. This could be one of the reasons why the average lifetime of $H_3O^+$ reported in literatures varies in a rather wide range.[51] For example, through the measurements of proton conductance,[49] the average lifetime was estimated to be 240 fs, whereas a higher value, by about one order of magnitude, was derived from dielectric relaxation data.[58] While the measurement of the low frequency (1200 $cm^{-1}$) in the vibrational spectrum of $H_3O^+$ requires a minimum lifetime of only 30 fs,[51] the one obtained from the measurement of $^{17}O$-induced proton relaxation in water and very dilute acids amounts to 2.2 ps.[59,60] In the present study, the average lifetime of $H_3O^+$ in the Eigen complex is within this range. It should be added that, in our model systems, the lack of continuous H-bond network connecting the first and second hydration shells could restrict the mobility of proton, whereas the inclusion of strong interaction between proton and polar environment could lead to a retardation of proton transfer events.[56] Our $\langle\tau_{H_9O_4^+}^{III,A}\rangle$ = 68.2 fs is, however, closer to the lowest limit, estimated from the low-frequency vibrational spectroscopy.[51]

**3.2.2 The $CF_3SO_3H$–$H_3O^+$–$H_2O$ complexes.** Fig. 6 shows examples of proton transfer profiles for the $CF_3SO_3H$–$H_3O^+$–$H_2O$ 1 : 1 : 1 complex, with snapshots of H-bond structures observed in the course of BOMD simulations. Three important elementary reactions were extracted from BOMD results and illustrated in Fig. 7 with all other results. For the $CF_3SO_3H$–$H_3O^+$–$H_2O$ 1 : 1 : 1 complexes, both large- and small-amplitude vibrations exist in the proton transfer profiles. In Fig. 6b, large-amplitude vibrations are seen, for example, between $t_1$ = 27 fs and $t_3$ = 420 fs, within which quasi-dynamic equilibria, followed by actual proton transfers in the reverse direction are seen in general. Small-amplitude vibrations are, for example, from $t_3$ = 420 fs to $t_4$ = 647 fs. Starting from structure **a** in Fig. 1, the H-bond proton ($H_2$* in Fig. 6c) moved in the course of BOMD simulations from O2 to O3, resulting in structure **A** in Fig. 6c. The proton transfer profile in Fig. 6a and the snapshots in Fig. 6c reveal an example of the H-bond structure reorganization from cyclic to linear. At $t_5$ = 750 fs, $H_6$* forms H-bond with an oxygen atom of $-SO_3H$, then structure **C** changes to structure **D**. Structures **D**, **E** and **F** show a possibility for proton transfer away from $-SO_3H$; whereas structure **G** for proton transfer in the reverse direction; forming $-SO_3H_2^+$ between $t_8$ = 1335 fs and $t_9$ = 1416 fs. The probability for proton transfer through the formation of $-SO_3H_2^+$ is higher for structure **c** in Fig. 3. Starting from structure **c**, $-SO_3H_2^+$ was generated right at the beginning of BOMD simulations. Snapshots in Fig. 6d reveal that structure **A** acts as a precursor and the proton transfer could be mediated by $-SO_3H_2^+$ in both directions; from structures **A** to **B** to **C**, as well as from structures **A** to **D** to **E**. Since there is no water molecule to stabilize the product

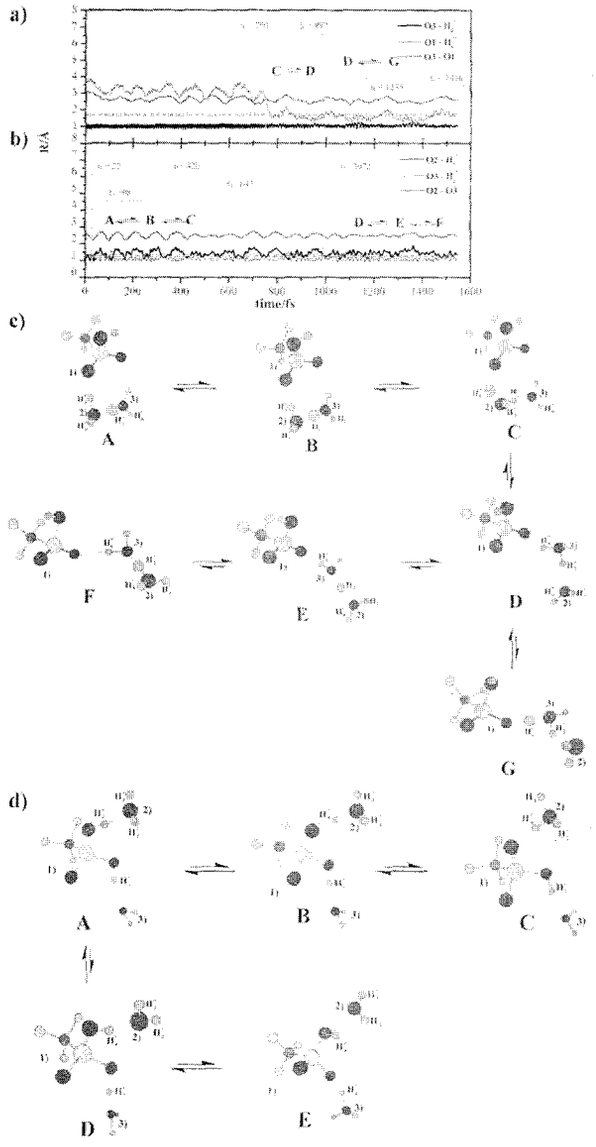


**Fig. 6** Examples of proton transfer profiles for the $CF_3SO_3H$–$H_3O^+$–$H_2O$ 1 : 1 : 1 complexes, with snapshots of H-bond structures observed in the course of BOMD simulations. (a)–(b) BOMD simulations starting from structure a in Fig. 1. (c)–(d) Snapshots of H-bond structures.

($H_3O^+$), both structures **C** and **E** return to structure **A**, as also recognized in the case of $H_7O_3^+$.

The results in Fig. 7 show that, due to a limited number of water molecules, the products in elementary reactions **I** and **II** were observed in short times. $\langle\tau_{1:1:1}^{\mathrm{I,C}}\rangle$ and $\langle\tau_{1:1:1}^{\mathrm{II,C}}\rangle$ are 10.1 and 9.3 fs, respectively, compared to the lifetimes of the precursors, $\langle\tau_{1:1:1}^{\mathrm{I,A}}\rangle$ and $\langle\tau_{1:1:1}^{\mathrm{II,A}}\rangle$, of 51.0 and 54.6 fs, respectively. For elementary reaction **I**, the quasi-dynamic equilibrium between the precursor and the transition state ($\langle\tau_{1:1:1}^{\mathrm{I,AB}}\rangle$) is 38.8 fs, with the average maximum proton transfer cycle time ($\langle\tau_{1:1:1}^{\mathrm{I,PTmax}}\rangle$) of 79.9 fs; whereas those of elementary reaction **II** are 25.3 and 95.8 fs, respectively. The values of $g_{1:1:1}^{\mathrm{I}}$ and $P_{1:1:1}^{\mathrm{I,forw}}$, as well as $g_{1:1:1}^{\mathrm{II}}$ and $P_{1:1:1}^{\mathrm{II,forw}}$ in Fig. 7, indicate that the degrees of coherence in elementary reactions **I** and **II** are comparable with $H_9O_4^+$, with a lower probability for proton transfer in the forward direction; $P_{1:1:1}^{\mathrm{I,forw}}$ and $P_{1:1:1}^{\mathrm{II,forw}}$ are only 0.2. Elementary reaction **III** in Fig. 7 involves proton transfer through $-SO_3H_2^+$. Although elementary reaction **III** possesses the highest degree of coherence, $g_{1:1:1}^{\mathrm{III}} = 0.8$, the probability for proton transfer from $-SO_3H_2^+$ and the lifetime of the product are the highest; $P_{1:1:1}^{\mathrm{III,forw}} = 0.4$ and $\langle\tau_{1:1:1}^{\mathrm{III,C}}\rangle = 23.9$ fs. These confirm the possibility that $-SO_3H_2^+$ could represent an effective transition state in proton transfer pathway at low hydration levels.[26]

For the $CF_3SO_3H$–$H_3O^+$–$H_2O$ 1 : 1 : 2 complexes, five important proton transfer elementary reactions could be extracted from BOMD results. The extension of the H-bond network in the vicinity of $-SO_3H$ could bring about both stabilization and destabilization effects to $H_3O^+$, depending upon the H-bond structures. Comparison of the results in Fig. 7 and 8 shows that, for elementary reaction **I**, the average lifetimes of the precursor ($\langle\tau_{1:1:2}^{\mathrm{I,A}}\rangle$), as well as the quasi-dynamic equilibrium ($\langle\tau_{1:1:2}^{\mathrm{I,ABC}}\rangle$), are increased when $H_3O^+$ is triply H-bonded; the former is 73.7 fs, and the latter is 29.0 fs. These are accompanied by an increase in the degree of coherence and a decrease in the average lifetime of the product, $g_{1:1:2}^{\mathrm{I}} = 0.8$ and $\langle\tau_{1:1:2}^{\mathrm{I,C}}\rangle = 7.8$ fs, as well as a decrease in the probability for proton transfer in the forward direction, $P_{1:1:2}^{\mathrm{I,forw}} = 0.1$.

Elementary reactions **II**, **III** and **IV** in Fig. 8 represent three possibilities for proton transfers along the linear H-bonds at $-SO_3H$. For elementary reaction **II**, the extension of the H-bond network, through the formation of the O–H···Ow H-bond, brings about higher stability to $H_3O^+$. This makes it difficult for $H_3O^+$ to transfer a proton to the adjacent water. Comparison of $P_{1:1:1}^{\mathrm{II,forw}}$ and $P_{1:1:2}^{\mathrm{II,forw}}$ in Fig. 7 and 8 shows that, due to an increase in the stability of $H_3O^+$ in elementary reaction **II**, the probability for proton transfer away from $-SO_3H$ is considerably decreased; structure **C** which is the product was rarely found in the course of BOMD simulations. Comparison of elementary reaction **III** in Fig. 7 and 8 reveals a similar trend, namely, the probability for $H_3O^+$ to protonate at $-SO_3H$ is reduced upon the Oh–Hh···Ow H-bond formation, with a shorter average lifetime of $-SO_3H_2^+$, $\langle\tau_{1:1:2}^{\mathrm{III,C}}\rangle = 11.7$ fs, compared to $\langle\tau_{1:1:1}^{\mathrm{III,A}}\rangle = 66.2$ fs. The elementary reaction **IV** shows a small probability to detect $-SO_3^-$ in the course of BOMD simulations, with $P_{1:1:2}^{\mathrm{IV,forw}} = 0.03$. In this case, large-amplitude vibration with $g_{1:1:2}^{\mathrm{IV}} \approx 1.0$, dominates and the charged product possesses very short average lifetime, $\langle\tau_{1:1:2}^{\mathrm{IV,C}}\rangle = 4.7$ fs. The stability of $H_3O^+$ and the degree of coherence in the H-bond are substantially reduced upon larger cyclic H-bond network formation; $\langle\tau_{1:1:2}^{\mathrm{V,A}}\rangle$ and $g_{1:1:2}^{\mathrm{V}}$ for elementary reaction **V** are 10.2 fs and 0.14, respectively. The values are close to those in $H_5O_2^+$. Since the average lifetimes of both precursor and product are small, the probability for proton transfer in the forward direction is the highest among the $CF_3SO_3H$–$H_3O^+$–$H_2O$ 1 : 1 : 2 complexes, with $P_{1:1:2}^{\mathrm{V,forw}} = 0.6$.

Due to a high degree of freedom in the $CF_3SO_3H$–$H_3O^+$–$H_2O$ 1 : 1 : 3 complexes, only linear H-bonds were observed in the course of BOMD simulations. The elementary reactions **I**, **II** and **III** in Fig. 9 represent three possibilities for proton transfer along the H-bond network

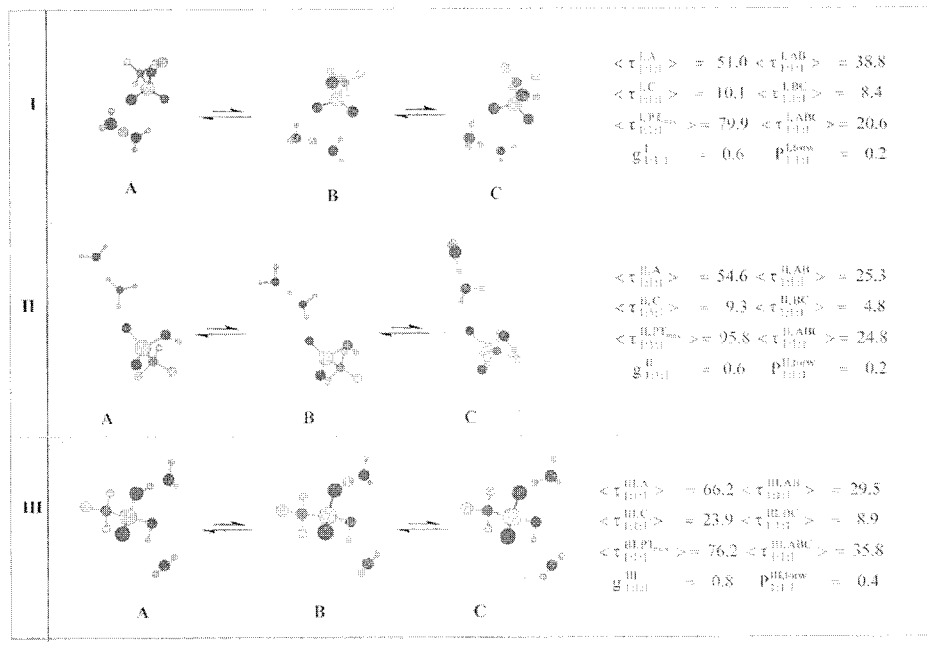

**Fig. 7** Important elementary reactions in proton transfer in the $CF_3SO_3H$–$H_3O^+$–$H_2O$ 1 : 1 : 1 complexes, obtained from BOMD simulations. The symbols are explained in details in the text.

passing through $-SO_3H$. Large-amplitude vibrations seem to dominate in elementary reactions **I** and **II**, with $g^{I}_{1:1:3}$ and $g^{II}_{1:1:3}$ of 0.8. Elementary reactions **I** and **II** show that when the H-bond network is well connected on both sides of $-SO_3H$, the stability of $H_3O^+$ is increased. This tends to reduce the probability for the proton transfers from $H_3O^+$ to $H_2O$, as well as from $H_3O^+$ to $-SO_3H$; both $P^{I,forw}_{1:1:3}$ and $P^{II,forw}_{1:1:3}$ are only about 0.1. The former reflects the possibility for proton transfer away from $-SO_3H$, and the latter for the formation of $-SO_3H_2^+$. Elementary reaction **III** reveals a quite high possibility for proton transfer through the formation of $-SO_3^-$, through an ion-pair complex similar to structure **e** in Fig. 2. The results in Fig. 9 indicate further that, for elementary reaction **III**, large-amplitude vibration dominates, with $g^{III}_{1:1:3} = 0.9$, and the probability for proton transfer in the forward direction is the highest among the $CF_3SO_3H$–$H_3O^+$–$H_2O$ 1 : 1 : 3 complexes, with $P^{III,forw}_{1:1:3} = 0.7$. The latter is slightly higher than $P^{V,forw}_{1:1:2}$.

## 4. Conclusions

Attempt has been made in the present work to study proton transfer reactions at a hydrophilic functional group in model Nafion®, using a theoretical method which takes into account the dynamics of formation and cleavage of covalent and H-bonds. Complexes formed from $CF_3SO_3H$, $H_3O^+$ and $H_2O$ were employed as model systems, from which the dynamics of an excess proton and proton defects at and in the vicinity of $-SO_3H$ were systematically studied, with the emphasis on how $-SO_3H$ facilitates or mediates proton transfer reactions at low hydration levels.

It was found in general that all characteristic H-bond structures and trends of proton transfer in the $H_3O^+$–$H_2O$ 1 : $n$ and $CF_3SO_3H$–$H_3O^+$–$H_2O$ 1 : 1 : $n$ complexes, $1 \leq n \leq 3$, could be predicted reasonably well by T-model, B3LYP/6-31G(d,p) and MP2/6-311++G(d,p) calculations. The theoretical results revealed possibilities for proton transfer along the H-bond network of water connecting the oxygen atoms of $-SO_3H$, as well as by relay-type mechanisms, in which proton hops across $-SO_3H$ through the formations of the $-SO_3H_2^+$ and $-SO_3^-$ transition states.

A series of BOMD simulations at 298 K was performed based on B3LYP/6-31G(d,p) calculations. Attention was focused on the precursors and transition states with H-bonds susceptible to proton transfers. Since the Zundel and Eigen complexes play the most important role in proton transfer reactions in aqueous solutions, their basic dynamic behavior was initially studied. It appeared that proton transfer in $H_5O_2^+$ depends strongly on the Oh–Hh···Ow H-bond separation, as well as its vibrational amplitude. Two extreme cases, namely, large- and small-amplitude vibrations, were analyzed and discussed in details based on proton transfer profiles. BOMD results showed that, due to the thermal energy fluctuation and coupled motions among H-bonds, a quasi-dynamic equilibrium between the Eigen and Zundel complexes could be established and considered to be one of the most important elementary reactions in the proton transfer process. Although our model systems lack of continuous H-bond network connecting the first and second hydration shells, the average lifetime of $H_3O^+$ in the Eigen complex is in reasonable agreement with the lowest limit estimated from low-frequency vibrational spectroscopy.

For the $CF_3SO_3H$–$H_3O^+$–$H_2O$ complexes, various temporary proton defects in H-bond structures were observed in the course of BOMD simulations. Due to the thermal energy fluctuation and dynamics at 298 K, proton transfer reactions at $-SO_3H$ seem to comprise various elementary reactions in

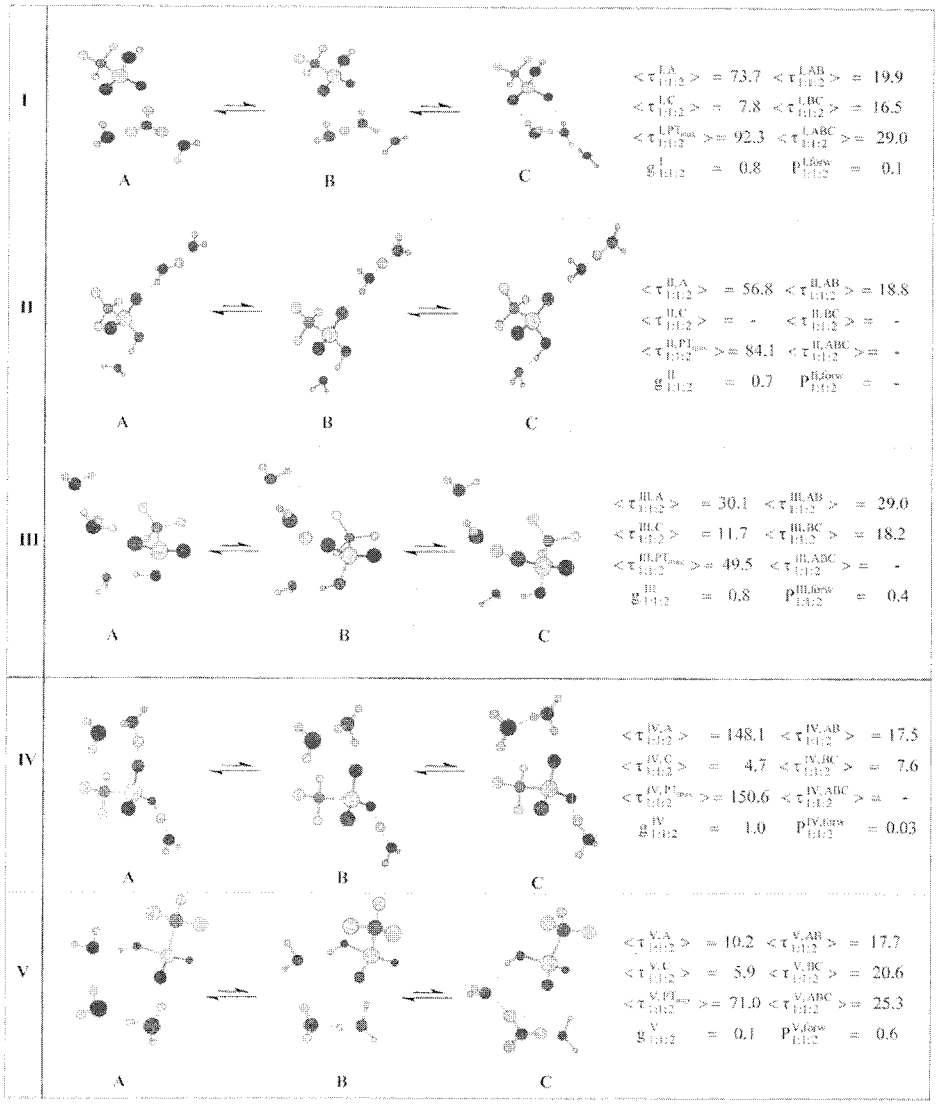

**Fig. 8** Important elementary reactions in proton transfer in the $CF_3SO_3H$–$H_3O^+$–$H_2O$ 1 : 1 : 2 complexes, obtained from BOMD simulations. The symbols are explained in details in the text.

quasi-dynamic equilibria. These prohibit proton transfer reactions from being concerted, and confirm the observations that the proton motion is too fast to be a rate-determining step. Due to large- and small-amplitude vibrations in H-bond separations, the internal conversions between covalent and H-bonds, similar to the Grotthuss mechanism, were concluded to form the general basis for proton transfer processes at $-SO_3H$. Attempt was also made to describe these proton-relay type mechanisms in terms of coherence and incoherence effects. BOMD simulations showed that the proton-relay type mechanisms could take place among $-SO_3H$, $H_3O^+$ and $H_2O$, providing some effective proton transfer pathways, through the formations of the $-SO_3^-$, $-SO_3H_2^+$ and $H_5O_2^+$ transition states. The analyses of the average lifetimes of the precursors and elementary reactions suggested that when the H-bond structures are right, in order that $-SO_3H$ could effectively function as a mediator in proton transfer reactions, the probabilities for the elementary reactions to proceed in the forward and reverse directions should be somewhat equivalent, otherwise the proton would be trapped at $-SO_3H$.

Finally, it should be emphasized that the present BOMD simulations focused on proton transfer processes at and in the proximity of a single $-SO_3H$ group, and within a narrow timescale. Therefore, H-bond structure reorganizations and molecular diffusions, which could contribute to proton conduction in different timescales, were not taken into account. It should be also added that the present theoretical investigations were performed at low hydration levels, in which the H-bond networks are not as extensive as in aqueous solutions, and strong interaction between proton and the polar environment could lead to a retardation of proton transfer. Therefore, direct comparisons between our model calculations and experiments seem not appropriate. However, some important insights, especially the interplays between local H-bond structures and dynamics, as well as the potential precursors and the proton transfer elementary reactions in an excess proton

 

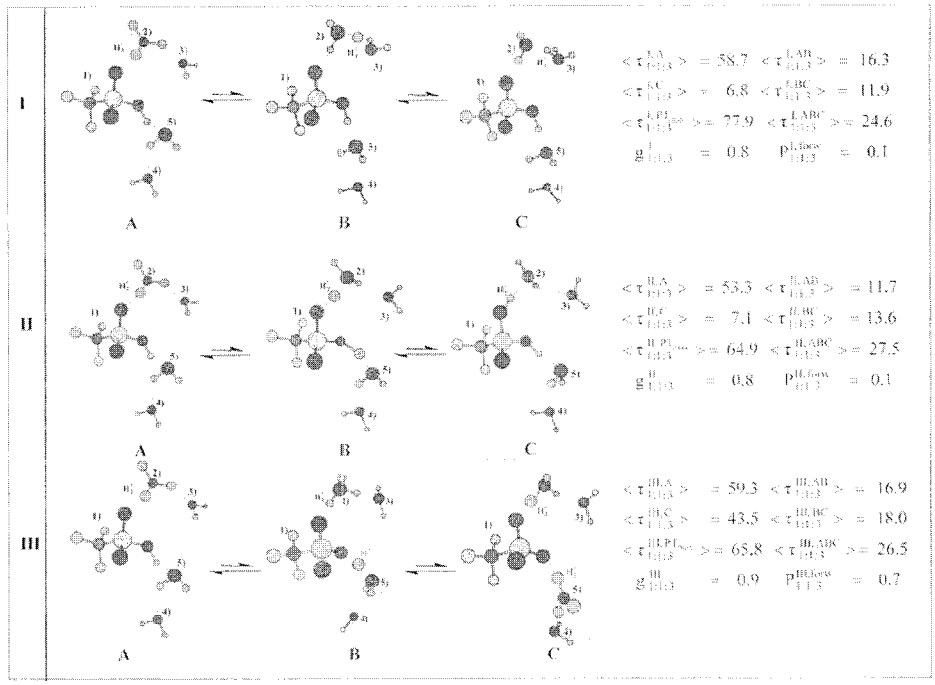

**Fig. 9** Important elementary reactions in proton transfer in the $CF_3SO_3H$–$H_3O^+$–$H_2O$ 1 : 1 : 3 complexes, obtained from BOMD simulations. The symbols are explained in details in the text.

condition, could be obtained. The present BOMD results also iterated that the equilibrium structures and energetic obtained from MM or *ab initio* geometry optimizations could not provide complete information on chemical reactions, especially the reaction pathways. It appeared that the theoretical methods and the analyses adopted in the present work could provide the practical basis for study of proton transfer reactions in larger H-bond systems. Based on similar approaches, progress has been made in our laboratory to include more hydrophilic functional groups and appropriate solvent effects in model systems of Nafion®.

## Acknowledgements

The authors would like to acknowledge financial support from the Thailand Research Fund (TRF); the Advanced Research Scholarship (BRG-4880008) for Prof. Kritsana Sagarik: the Royal Golden Jubilee (RGJ) PhD Program, Grant No. PHD/0110/2548 for Mayuree Phonyiem; Grant No. PHD/0071/2547 for Sermsiri Chaiwongwattana; Grant No. PHD/0121/2549 for Charoensak Lao-ngam. Linux cluster facilities have been provided by School of Mathematics and School of Chemistry, SUT, as well as the Thai-Grid Project, National Electronics and Computer Technology Center (NECTEC) and National Nanotechnology Center (NANOTEC), Thailand.

## References

1 J. Larminie and A. Dicks, *Fuel Cell Syst.*, John Wiley & Sons Ltd, Chichester, 2001.
2 C. A. Vincent and B. Scrosati, *Modern Batteries: An introduction to electrochemical power sources*, John Wiley & Sons Ltd, New York, 1997.
3 T. Koppel, *Powering the Future: The ballard fuel cell and the race to change the world*, John Wiley & Sons Ltd, New York, 1999.
4 J. T. Hinatsu, M. Mizuhata and H. Takenaka, *J. Electrochem. Soc.*, 1994, **141**, 1493.
5 K. A. Mauritz and R. B. Moore, *Chem. Rev.*, 2004, **104**, 4535.
6 T. D. Gierke, G. E. Munn and F. C. Wilson, *J. Polym. Sci. Polym. Phys.*, 1981, **19**, 1687.
7 S. J. Paddison, *Annu. Rev. Mater. Res.*, 2003, **33**, 289.
8 K. D. Kreuer, *Chem. Mater.*, 1996, **8**, 610.
9 K. D. Kreuer, S. J. Paddison, E. Spohr and M. Schuster, *Chem. Rev.*, 2004, **104**, 4637.
10 S. J. Paddison and T. Zawodzinski, Jr, *Solid State Ionics*, 1998, **115**, 333.
11 S. J. Paddison, L. R. Pratt and T. A. Zawodzinski, Jr, *J. New Mater. Electrochem. Syst.*, 1999, **2**, 183.
12 M. Laporta, M. Pegoraro and L. Zanderighi, *Phys. Chem. Chem. Phys.*, 1999, **1**, 4619.
13 A. Vishnyakov and A. V. Neimark, *J. Phys. Chem. B*, 2000, **104**, 4471.
14 R. Buzzoni, S. Bordiga, G. Ricchiardi, G. Spoto and A. Zecchina, *J. Phys. Chem.*, 1995, **99**, 11937.
15 A. Zecchina, F. Geobaldo, G. Spoto, S. Bordiga, G. Ricchiardi, R. Buzzoni and G. Petrini, *J. Phys. Chem.*, 1996, **100**, 16584.
16 S. J. Paddison, G. Bender, K. D. Kreuer, N. Nicoloso and T. A. Zawodzinski, Jr, *J. New Mater. Electrochem. Syst.*, 2000, **3**, 293.
17 N. G. Boyle, V. J. McBrierty and A. Eisenberg, *Macromolecules*, 1983, **16**, 80.
18 S. J. Paddison, L. R. Pratt, T. A. Zawodzinski, Jr and D. W. Reagor, *Fluid Phase Equilib.*, 1998, **150**, 235.
19 S. J. Paddison, L. R. Pratt and T. Zawodzinski, Jr, *J. Phys. Chem. A*, 2001, **105**, 6266.
20 S. J. Paddison, *J. New Mater. Electrochem. Syst.*, 2001, **4**, 197.
21 M. Eikerling, S. J. Paddison, L. R. Pratt and T. A. Zawodzinski, Jr, *Chem. Phys. Lett.*, 2003, **368**, 108.
22 M. Cappadonia, J. W. Erning, S. M. S. Niaki and U. Stimming, *Solid State Ionics*, 1995, **77**, 65.
23 S. J. Paddison and J. A. Elliott, *J. Phys. Chem. A*, 2005, **109**, 7583.

24 S. J. Paddison and J. A. Elliott, *Phys. Chem. Chem. Phys.*, 2006, **8**, 2193.
25 S. J. Paddison and J. A. Elliott, *Solid State Ionics*, 2006, **177**, 2385.
26 V. A. Glezakou, M. Dupuis and C. J. Mundy, *Phys. Chem. Chem. Phys.*, 2007, **9**, 5752.
27 J. M. Hermida-Ramon and G. Karlstroem, *J. Mol. Struct. (THEOCHEM)*, 2004, **712**, 167.
28 A. Botti, F. Bruni, S. Imberti, M. A. Ricci and A. K. Soper, *J. Mol. Liquid*, 2005, **117**, 77.
29 M. D. Newton, *J. Chem. Phys.*, 1978, **67**, 5535.
30 K. P. Sagarik and B. M. Rode, *Chem. Phys.*, 2000, **260**, 159.
31 K. P. Sagarik, S. Chaiwongwattana and P. Sisot, *Chem. Phys.*, 2004, **306**, 1.
32 K. P. Sagarik and S. Dokmaisrijan, *J. Mol. Struct. (THEOCHEM)*, 2005, **718**, 31.
33 K. Sagarik and S. Chaiyapongs, *Biophys. Chem.*, 2005, **117**, 18.
34 N. Deeying and K. Sagarik, *Biophys. Chem.*, 2007, **125**, 72.
35 K. D. Kreuer, *Solid State Ionics*, 2000, **136**, 149.
36 U. W. Schmitt and G. A. Voth, *J. Chem. Phys.*, 1999, **111**, 9361.
37 K. P. Sagarik and R. Ahlrichs, *J. Chem. Phys.*, 1987, **86**, 5117.
38 K. P. Sagarik, V. Pongpituk, S. Chiyapongs and P. Sisot, *Chem. Phys.*, 1991, **156**, 439.
39 K. P. Sagarik, *J. Mol. Struct. (THEOCHEM)*, 1999, **465**, 141.
40 K. P. Sagarik and E. Spohr, *Chem. Phys.*, 1995, **199**, 73.
41 K. P. Sagarik and P. Asawakun, *Chem. Phys.*, 1997, **219**, 173.
42 M. J. Frisch, G. W. Trucks, H. B. Schlegel, G. E. Scuseria, M. A. Robb, J. R. Cheeseman, V. G. Zakrzewski, J. A. Montgomery, Jr, R. E. Stratmann, J. C. Burant, S. Dapprich, J. M. Millam, A. D. Daniels, K. N. Kudin, M. C. Strain, O. Farkas, J. Tomasi, V. Barone, M. Cossi, R. Cammi, B. Mennucci, C. Pomelli, C. Adamo, S. Clifford, J. Ochterski, G. A. Petersson, P. Y. Ayala, Q. Cui, K. Morokuma, P. Salvador, J. J. Dannenberg, D. K. Malick, A. D. Rabuck, K. Raghavachari, J. B. Foresman, J. Cioslowski, J. V. Ortiz, A. G. Baboul, B. B. Stefanov, G. Liu, A. Liashenko, P. Piskorz, I. Komaromi, R. Gomperts, R. L. Martin, D. J. Fox, T. Keith, M. A. Al-Laham, C. Y. Peng, A. Nanayakkara, M. Challacombe, P. M. W. Gill, B. Johnson, W. Chen, M. W. Wong, C. Gonzalez and J. A. Pople, *GAUSSIAN 03 (Revision D.1)*, Gaussian, Inc.,Wallingford, CT, 2005.
43 P. B. Balbuena and J. M. Seminario, *Theoretical and Computational Chemistry 7, Molecular dynamics; from classical to quantum methods*, Elsevier, Amsterdam, 1999.
44 C. J. Cramer, *Essentials of Computational Chemistry: Theory and models*, John Wiley & Sons, Ltd, 2002.
45 D. C. Young, *Computational Chemistry: A practical guide for applying techniques to real world problems*, Wiley Interscience, New York, 2001.
46 R. N. Barnett and U. Landman, *Phys. Rev.*, 1993, **B48**, 2081.
47 X. Jing, N. Troullier, D. Dean, N. Binggeli, J. R. Chelikowsky, K. Wu and Y. Saad, *Phys. Rev.*, 1994, **B50**, 122.
48 A. R. Leach, *Molecular Modelling: Principles and applications*, Longman, Edinburgh, 1996.
49 B. E. Conway, J. O. M. Bockris and H. Linton, *J. Chem. Phys.*, 1956, **24**, 834.
50 N. Agmon, *Chem. Phys. Lett.*, 1995, **244**, 456.
51 P. A. Giguere, *J. Chem. Educ.*, 1979, **56**, 571.
52 JMOL website http://jmol.sourceforge.net/.
53 X. Duan and St. Scheiner, *J. Mol. Struct.*, 1992, **270**, 173.
54 R. Janoscheck, *J. Mol. Struct.*, 1994, **231**, 45.
55 C. J. D. von Grotthuss, *Annu. Chim.*, 1806, **58**, 54.
56 K. D. Kreuer, *Solid State Ionics*, 1997, **94**, 55.
57 M. Eigen and L. De Maeyer, *Proc. R. Soc.*, 1958, **A247**, 505.
58 M. Eigen, *Angew. Chem.*, 1963, **75**, 489.
59 R. E. Glick and K. C. Tewari, *J. Chem. Phys.*, 1966, **44**, 546.
60 S. W. Rabideau and H. G. Hetch, *J. Chem. Phys.*, 1967, **47**, 544.

 